

Thickness-Dependent Ru Exchange Spring at $\text{La}_{0.7}\text{Sr}_{0.3}\text{MnO}_3$ – SrRuO_3 Interface

Martin M. Koch, Lukas Bergmann, Stefano Agrestini, Igor Maznichenko, Ingrid Mertig, Andreas Herklotz, Sujit Das, Diana A. Rata, and Kathrin Dörr*

The conducting oxide ferromagnets SrRuO_3 (SRO) and $\text{La}_{0.7}\text{Sr}_{0.3}\text{MnO}_3$ (LSMO) form a Ru exchange spring at a coherent low-interdiffusion interface grown on TiO_2 -terminated SrTiO_3 (STO)(001) substrates as SRO(*d*)/LSMO/STO(001) bilayers. Field- and temperature-dependent magnetization data with systematically varied thickness *d* of SRO from 7 to 18 unit cells (uc) indicate a thickness of 10–14 uc of the exchange spring which governs magnetic switching and causes thickness-dependent field-cooling effects. Mn L_3 edge X-ray magnetic circular dichroism (XMCD) data reveal the dominating in-plane orientation of interfacial spins. In low magnetic fields, noncoplanar, topologically nontrivial spin textures arise and can be switched, driven by the Zeeman energy of the LSMO layer.

1. Introduction

Magnetic order at interfaces often deviates from that of bulk materials. For coherent interfaces of perovskite-type oxides ABO_3 with metals A and B, the interfacial magnetic order is yet often unknown. Like at interfaces between metallic ferromagnets, magnetic anisotropy, exchange, and Dzyaloshinskii–Moriya (DM) couplings across the interface are essential for the interfacial spin structure.^[1,2] There are, however, more chemical and structural parameters affecting interfacial magnetic coupling and anisotropy than in metals. Recently, experimental evidence has been accumulated, revealing a crucial impact of the collective rotations of oxygen octahedrons (OOR) on interfacial magnetic anisotropy: near an

interface, the rotation pattern can be different from both components' bulk rotation patterns^[3] and cause altered interfacial magnetic anisotropy.^[4,5] The exchange coupling depends on OOR and on the atomic interface composition (e.g., see the study by Das et al.^[6]). This includes effects of the chemical termination of both components (ABO_3 -A * B * O_3 can be terminated like AO-B * O_2 or BO_2 -A * O), intermixing and vacancy accumulation.^[7] Strong DM coupling is expected at interfaces containing heavier metal ions; it has been suggested for the SrIrO_3 – SrRuO_3 (SRO) interface.^[8,9]

Recently, the control of DM interaction in SRO by interfacing with ferroelectric BaTiO_3 has been suggested.^[10] In addition, there are electronic degrees of freedom: charge transfer across the interface may alter or induce magnetic moments,^[11] and orbital occupation of d orbitals may deviate from bulk,^[12,13] resulting in altered exchange coupling.


These many parameters have, thus far, hampered the development of a comprehensive view, enabling the general control of oxide interfacial spin textures. However, there are a few well-studied interfaces. The earliest among them was $\text{La}_{0.7}\text{Sr}_{0.3}\text{MnO}_3$ – SrTiO_3 (LSMO–STO) between a ferromagnet and a diamagnet; this interface is essential for magnetic tunnel junctions with the (near) half-metal LSMO.^[14] It shows an undesirable loss of ferromagnetic order at the interface with increasing temperature, related to intermixing and charge transfer.^[15] The latter can induce a magnetic Ti moment.^[11] Another well-studied example is LSMO– BiFeO_3 ,^[16,17] where the magnetoelectric antiferromagnet BiFeO_3 is used for an electrically controllable exchange bias and shows an induced interfacial Fe magnetic moment antiparallel to Mn.

In this work, the investigated coherent interface is between two ferromagnets, LSMO and SRO. This interface has received substantial interest as in previous studies,^[6,7,18–23] mostly because of its very strong Mn–O–Ru exchange coupling which is antiferromagnetic. There is a strong exchange bias effect on LSMO switching, which depends—even in sign—on the “frozen-in” orientation of interfacial Ru magnetic moments.^[22] The freezing of Ru spins results from the strong increase in SRO magnetocrystalline anisotropy at low temperatures. Early work assumed collinear ferromagnetic order in both components, however, an enlarged in-plane Ru magnetic moment at interfaces has been derived by Kim et al. from neutron depolarization data.^[23] In the bulk of SRO layers grown at the coherent in-plane lattice parameter of 3.905 Å, Ru has a canted out-of-plane

M. M. Koch, L. Bergmann, Dr. I. Maznichenko, Prof. I. Mertig, Dr. A. Herklotz, S. Das, Dr. D. A. Rata, Prof. K. Dörr
Institute of Physics
Martin Luther University Halle-Wittenberg
Halle 06099, Germany
E-mail: kathrin.doerr@physik.uni-halle.de

Dr. S. Agrestini
ALBA Synchrotron Light Source
Cerdanyola del Vallès, Barcelona E-08290, Spain

Prof. I. Mertig
Max Planck Institute of Microstructure Physics
Weinberg 2, Halle 06120, Germany

 The ORCID identification number(s) for the author(s) of this article can be found under <https://doi.org/10.1002/pssb.201900616>.

© 2020 The Authors. Published by WILEY-VCH Verlag GmbH & Co. KGaA, Weinheim. This is an open access article under the terms of the Creative Commons Attribution-NonCommercial License, which permits use, distribution and reproduction in any medium, provided the original work is properly cited and is not used for commercial purposes.

DOI: 10.1002/pssb.201900616

orientation.^[24] Therefore, the existence of an interfacial exchange spring was suggested.^[23] Exchange spring formation was also considered for other oxide interfaces,^[24] including LSMO/La_{0.7}Sr_{0.3}CoO₃.^[25] In our recent work,^[6] we demonstrate the existence of different types of LSMO–SRO interfaces in coherent LSMO/SRO bilayers on TiO₂-terminated STO(001) substrates. They form depending on chemical interface termination and growth sequence. The case of SRO/LSMO/STO(001) samples shows dominating MnO₂–SRO interface termination and very strong antiferromagnetic Mn–Ru coupling across the interface, in agreement with density functional theory calculations. For this type of bilayer, an exchange spring in SRO at the interface has been derived. Here, we analyze the exchange spring characteristics depending on SRO layer thickness using magnetization measurements. We suggest a configuration of the interfacial spin structure and discuss its impact on magnetic switching as well as further implications of such spin structures.

2. Results and Discussion

In **Figure 1**, the spin configuration of the exchange spring in LSMO–SRO bilayers is presented as a starting point; it had been derived in our previous work.^[6] At the interface, the 180° antiferromagnetic exchange coupling of Mn and Ru moments is “rigid” in the applied fields (<5 T). The LSMO layer has a collinear ferromagnetic orientation of Mn moments. The SRO moments are oriented in plane at the interface, whereas with increasing distance from the interface, the out-of-plane canting of Ru moments develops, which is typical for strained bulk-like SRO/STO(001) ($a = 3.905 \text{ \AA}$). The canting angle depends on temperature as a consequence of minimizing the sum of the magnetocrystalline anisotropy energy and magnetostatic energy.^[26] This “relaxed state” of the exchange spring is present if the applied in-plane magnetic field (H) is smaller than a switching field (H_s). Upon application of a larger field $H > H_s$ (right panel of

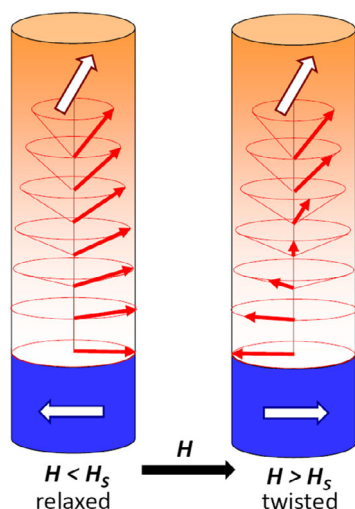


Figure 1. Scheme of the exchange spring at the SRO (top, red)/LSMO (bottom, blue) interface in an in-plane magnetic field. The relaxed state in small fields below the switching field H_s (left) and the twisted state in fields above H_s .

Figure 1), the magnetization of LSMO is oriented along the field direction. Due to the much larger magnetic anisotropy of bulk-like SRO, the magnetization of the upper part of the (sufficiently thick) SRO layer is unchanged, apart from a weak rotation toward the field direction. The interfacial Ru moments remain coupled to LSMO, forming a twisted exchange spring with the upper part of the layer. This arrangement of magnetic moments in the in-plane field is noncoplanar. The required switching field between the magnetic structures in the left and right panels of **Figure 1**, i.e., between relaxed and twisted states of the exchange spring, is of the order of 10 mT.^[6] Relaxing or twisting the Ru exchange spring is driven by the balance of magnetic anisotropy energy plus the exchange energy in SRO and the bilayer’s Zeeman energy in the applied field which is dominated by the LSMO layer. (The latter has negligible magnetic anisotropy energy in comparison with SRO.) We note that the presence of an exchange spring in SRO implies strong suppression of magnetic anisotropy at the interface, which will be discussed later. Second, the in-plane orientation of Ru moments at the interface will be justified in the discussion of **Figure 6**. The interfacial spin order in SRO resembles a Bloch wall with gradually increasing out-of-plane canting (**Figure 1**). An interesting question which remains presently unanswered concerns possible chirality of the Ru spin rotation in the exchange spring. Chirality might be induced by Dzyaloshinskii–Moriya interaction in the interface near SRO.

In the following, the cooling-field-dependent magnetization behavior resulting from different thicknesses of the SRO layer is discussed step wise. It is important to be aware of the fact that the applied magnetic field (<5 T) is not large enough to reach a domain-free state of the SRO layer. Therefore, the measured magnitudes of magnetization do not belong to a domain-free state; hence, all observed changes are smaller than those expected for a laterally uniform magnetization.

For the bilayer with the thinnest SRO top layer [7 unit cell (uc) SRO and 9 uc LSMO], the magnetic hysteresis loop $M(H)$ measured along an in-plane [100] direction at 10 K after field cooling in 3 T and the temperature-dependent magnetization $M(T)$ warming curve after cooling in 0.5 T or 3 T are shown in **Figure 2**. The hysteretic behavior of $M(H)$ is weak (**Figure 2a**), with small coercive fields of $10 \pm 2 \text{ mT}$ (inset of **Figure 2a**). No transition in larger fields up to 5 T has been observed. The horizontal line marks the saturated magnetic moment expected for 9 uc LSMO with collinear ferromagnetic order ($3.7 \mu_B/\text{Mn}$). The $M(H)$ loop can be understood in a way that the Ru spins reversibly, rotating toward the field direction, whereas the interface retains the antiferromagnetic coupling of SRO and LSMO. After reduction of the field, the rotation of Ru spins is fully reversible. Reversibility is also shown in temperature-dependent data, irrespective of the cooling field (0.5 or 3 T); subsequently measured $M(T)$ warming curves are identical within the error range (**Figure 2b**). This again indicates the absence of any “frozen-in” spins which is in contrast to the case of thicker SRO layers (discussed next). $M(T)$ presents another surprising feature: no transition at the Curie temperature of SRO (below 150 K) is detectable. The ordering of Ru spins may occur rather gradually in a temperature interval. According to density functional theory calculations of the exchange coupling strength between Ru and Mn,^[6] the MnO₂–SrO-terminated interface has an extremely large next-neighbor coupling constant of $J = 13 \text{ meV}$, comparable

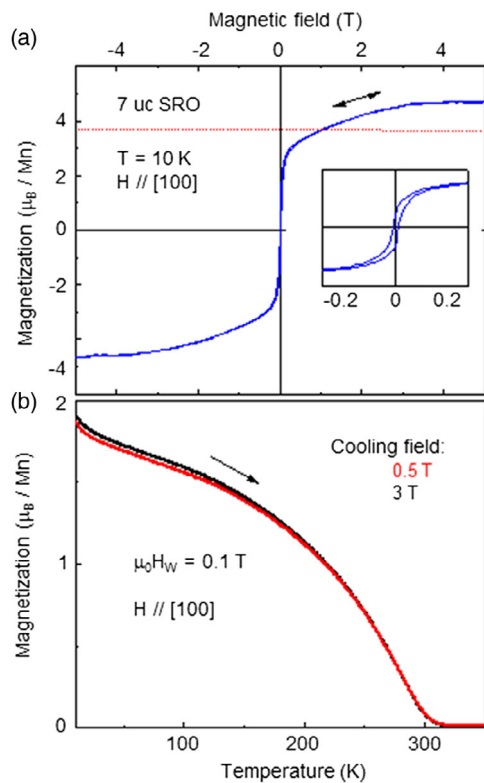


Figure 2. a) Field-dependent and b) temperature-dependent magnetizations (along an in-plane 100 direction) of a sample with 7 uc SRO. The dashed red line marks the saturated magnetization of the 9 uc LSMO layer alone.

with the internal coupling in LSMO. We speculate that this may drive Ru spin ordering at the interface first, possibly even above the bulk T_c of SRO. Subsequently, it gradually extends into the SRO layer during cooling.

The case of the next-thicker SRO layer (10 uc) is shown in **Figure 3**. While the $M(H)$ loop up to 5 T shows again weak hysteresis and nearly coincides with the loop for 7 uc SRO (**Figure 2a**), coercive fields are slightly larger and, now, an impact of the cooling field is clearly visible (**Figure 3a**). Cooling in 5 T (−5 T) aligns the majority of Ru spins with the in-plane field, causing an exchange-bias field of $\mu_0 H_{EB} = 7.5$ mT (−8.1 mT) for the reversal of LSMO magnetization (plus the coupled interfacial SRO). In contrast, the cooling field of 1 T (−1 T) is not sufficient to align most Ru spins in the field direction, but they align antiparallel to Mn spins and the applied field, causing an exchange-bias field of $\mu_0 H_{EB} = -17$ mT (16.8 mT), i.e., of opposite sign. These findings qualitatively agree with the cooling-field-dependent exchange bias reported by Ke et al. in bilayers of larger thicknesses.^[22] The coercive fields coincide with the switching fields H_s for relaxing the exchange spring after application of a large field. In agreement with the presence of frozen-in Ru spins, the $M(T)$ measurements (**Figure 3b**) reveal an impact of the cooling field, too. The magnetization was measured both during cooling in several different fields, shown in **Figure 3b**, and during subsequent warming in 0.1 T. The T_c of SRO is visible as the splitting point of cooling and warming

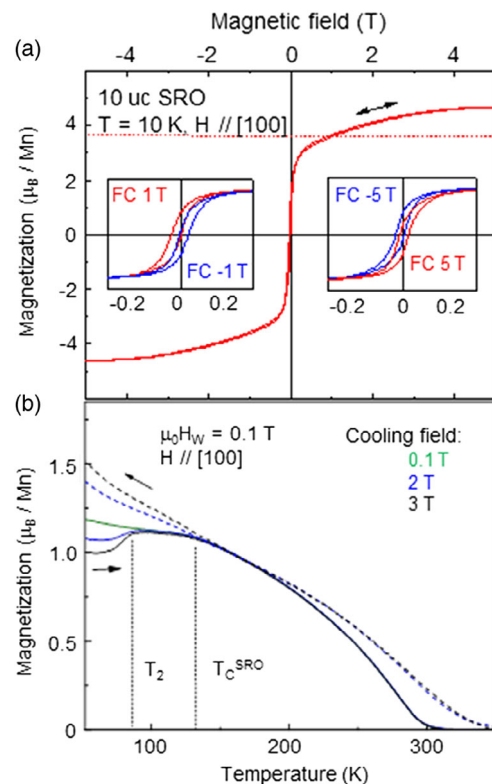


Figure 3. a) Field-dependent and b) temperature-dependent magnetizations after field cooling in the indicated fields (along an in-plane 100 direction) of a sample with 10 uc SRO. b) contains data measured during cooling, too (dashed lines). For 0.1 T, cooling and warming curves coincide.

curves near 140 K. There is a kink in warming curves near $T_2 \approx 80$ K where all warming curves meet. (This cannot be the SRO Curie temperature, as will be clearer below: samples with thicker SRO layers show both anomalies at T_2 and T_c^{SRO} in a distinct way, as shown in **Figure 4b**.) As a general observation from $M(T)$, the larger the cooling field, the lower the magnetization at 10 K after reducing the field to 0.1 T. This is a consequence of the frozen-in Ru spins aligned with the field during cooling: the 10 uc SRO layer is thick enough to keep its upper part aligned due to the large magnetic anisotropy at 10 K, whereas the exchange spring relaxes and reverses the low-anisotropy LSMO layer. This also leads to the origin of the T_2 anomaly: when starting the warming measurement at $T < T_2$, the LSMO magnetization points to a negative direction after cooling in large fields (3 T), whereas at the meeting point with the 0.1 T curve, it must be back to the positive direction which is present in the low-field (0.1 T) measurements during cooling and warming. Hence, a 180° reorientation of LSMO takes place below T_2 , driven by the Zeeman energy and the drop of SRO magnetic anisotropy with increasing temperature. This hypothesis is further supported as follows, where T_2 depending on the warming field is analyzed (**Figure 5b**). Note again that domains must be present in addition to the interfacial exchange spring, because the magnitude of the switching magnetization is much too small for a laterally uniform layer magnetization; the described mechanism

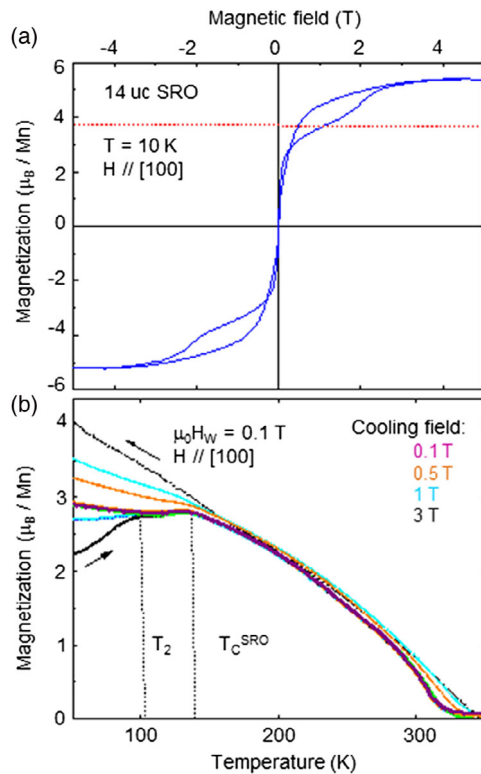


Figure 4. a) Field-dependent and b) temperature-dependent magnetizations after field cooling in the indicated fields (along an in-plane 100 direction) of a sample with 14 uc SRO. Data measured during cooling are included as dashed lines. For 0.1 T, cooling and warming curves coincide.

takes place in a fraction of the bilayer volume. Finally, we consider the even thicker SRO top layer of 14 uc (Figure 4). $M(T)$ curves resemble those of the 10 uc SRO sample (Figure 3b). In addition, a clear kink is now visible at the SRO Curie temperature of ≈ 140 K. The second anomaly appears at $T_2 = 105$ K.

Figure 5a,b shows data on the reorientation transition at T_2 for the impact of the SRO layer thickness (Figure 5a) and the magnetic field (H_w) applied during $M(T)$ warming runs (Figure 5b). For 7 uc SRO, no T_2 exists ($T_2 = 0$). For 14–20 uc SRO, T_2 seems to saturate near 115 K in 0.1 T for 9 uc LSMO. We insert an additional point with slightly thinner LSMO of 8 uc to visualize the possible scattering of T_2 values among samples; naturally, the T_2 value for 8 uc LSMO must be larger than for 9 uc. For 10 uc SRO, the exchange spring is distinctly weaker than for thicker SRO, allowing Zeeman energy to drive the LSMO reorientation at lower temperature (≈ 85 K). As T_2 saturates above 14 uc (5.5 nm) SRO, it seems to be the maximum thickness of the exchange spring. In agreement with the Zeeman energy argument, a larger measuring field reduces T_2 linearly within a certain range of field and temperature (Figure 5b). This linear trend cannot go on to low temperatures (like 10 K), as it does not include the growth of SRO magnetic anisotropy. The slope of $T_2(H_w)$ is larger, the thicker the LSMO layer is, in agreement with the Zeeman energy change. Curves for the same SRO thickness (of 10 uc) and different LSMO thicknesses meet at the same point for $H_w = 0$, as the

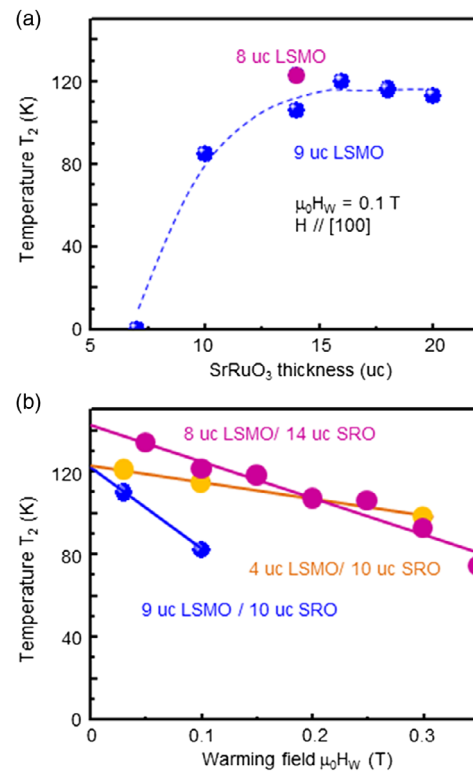


Figure 5. Spin reorientation temperature T_2 as a function of a) SRO thickness and b) magnetic field during temperature-dependent magnetization measurement.

SRO exchange spring is identical. In contrast, the thicker SRO layer (14 uc) has a larger extrapolated T_2 for $H_w = 0$. These observations are consistent with our interpretation given earlier.

X-ray magnetic circular dichroism (XMCD) magnetization loops of Mn recorded at 60 K perpendicular to the film plane (along [001]) (Figure 6a) and in “grazing incidence” (20°) “along” [100] (Figure 6b) for a 14 uc SRO/9 uc LSMO sample support the exchange spring configuration introduced earlier. (Ru XMCD hysteresis loops have been reported in the study by Das et al.^[6]) The out-of-plane loop (Figure 6a) is essentially that of Mn spins rotating out of the film plane in the vertical field. As a consequence of the dominating positive Ru spin direction after field cooling in 3 T, the Mn hysteresis loop runs with opposite sense, showing a small negative remanence. The remanent out-of-plane magnetization is very small, below 10% of the saturated value. As the remanence of Ru spins is large^[6] and Mn and Ru are rigidly coupled at the interface, domains can be excluded as the source of the small out-of-plane Mn remanence. Therefore, Mn spins lie essentially in the film plane. This allows us to conclude on interfacial Ru spins which must lie in the film plane, too, as a consequence of the very strong antiferromagnetic Mn–Ru coupling. For the in-plane Mn hysteresis (Figure 6b), one notes the very narrow loop at 60 K, with coercive fields of < 10 mT, which is below the error of the field measurement. The Mn spin reversal occurs when the field-dependent Zeeman energy of LSMO is not large enough to keep the exchange spring twisted.

Spin structures like that in the twisted exchange spring (Figure 1, right panel) may induce topological and magnetoelectric

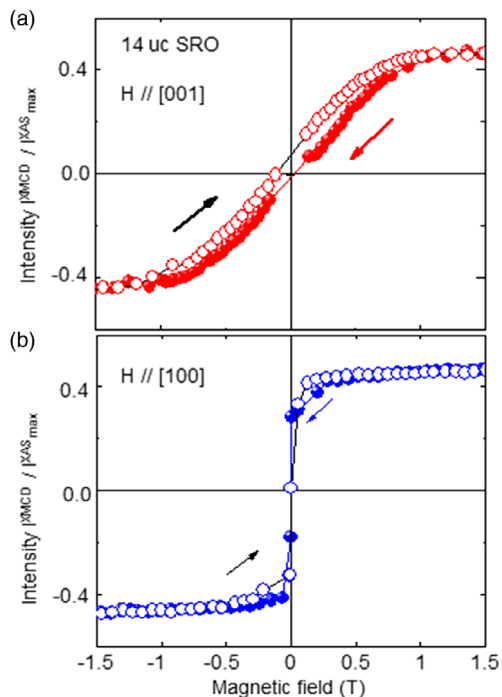


Figure 6. Mn-XMCD magnetization loops measured at 60 K along the a) out-of-plane [001] direction and an b) in-plane [100] direction (under 20° tilt) at the Mn L_3 edge absorption maximum. Intensity normalized to the value at the absorption maximum.

phenomena. The twisted spin configuration fulfills the criterion of Nagaosa et al. for being topologically nontrivial, which requires neighboring spins to be noncoplanar, i.e., $(\mathbf{S}_i \times \mathbf{S}_j) \cdot \mathbf{S}_k \neq 0$.^[27] Electrical transport effects like the topological Hall effect might occur. At present, the question on chirality of the twisted exchange spring is open; sufficient spin-orbit coupling in SRO would be able to induce DM interaction associated with chirality. There is increasing evidence for substantial DM interaction in SRO in the recent study by Wang et al.^[10] and references therein. We note that the magnitude of the field required to twist the exchange spring can be tuned by the thickness of the coupled LSMO layer which drives the switching by Zeeman energy. In contrast, the twisted exchange spring would be associated with electric polarization according to the relation introduced by Katsura et al., $\mathbf{P} \propto \mathbf{e}_{ij} \times (\mathbf{S}_i \times \mathbf{S}_j)$ with the electric polarization vector \mathbf{P} , neighboring spins \mathbf{S}_i and \mathbf{S}_j , and their connecting unit vector \mathbf{e}_{ij} .^[28] This is one of the well-known driving mechanisms of type II (bulk) multiferroics. A Bloch wall-type spin arrangement causes no polarization, but the additional gradual out-of-plane canting of Ru spins results in nonzero polarization. As SRO is a good conductor, polarization screening is expected to occur. This hampers polarization control by an electric field in the present samples, but if an insulating oxide ferromagnet would form a similar exchange spring, this may open another pathway for electric control of interfacial spin structures.

Why does SRO form an exchange spring? One necessary precondition is strong interfacial exchange coupling. Density functional theory calculations have shown a decisive impact of the chemical interface termination on coupling strength, with

very strong coupling at an (interdiffusion-free) MnO_2 -terminated interface and moderate coupling at an ideal RuO_2 -terminated interface.^[6] Hence, depending on chemical composition of the interface, the coupling between layers varies substantially. Our SRO/LSMO/STO(001) films show dominating MnO_2 termination with moderate intermixing,^[6] providing the strong coupling needed for an exchange spring. The second precondition is sufficiently small magnetic anisotropy in the interface near SRO. This is in striking contrast with the large bulk magnetocrystalline anisotropy of SRO. Therefore, the logical consequence is a strongly reduced interfacial anisotropy in SRO. We speculate that a structural instability of SRO between an orthorhombic and a tetragonal phase is involved such that SRO has a tetragonal structure at the interface and reduced anisotropy in an elastic “crossover range,” connecting the orthorhombic top part of thicker (≥ 14 uc) SRO films. The difference between the two structural phases manifests itself in the OOR.^[29,30] These rotations are likely to evolve gradually from the interface into the depth of the SRO layer, supporting the idea of a range with weak anisotropy, as easy axes change directions between the two phases. The tetragonal SRO phase is well known to appear in the following cases: 1) under a coherent tensile strain of $\approx 1\%$,^[29] 2) under a volume increase of 1–2%,^[31] and 3) in superlattices with ultrathin SRO layers and $\text{Pr}_{0.7}\text{Ca}_{0.3}\text{MnO}_3$ as the second component.^[32] The coherent strain of SRO in our bilayers is weakly compressive on STO(001), excluding case (1). An interfacial increase in the unit cell volume by 1–2% is easily possible, if some vacancies exist at the interface. Transfer of octahedral rotations between LSMO and SRO, probably underlying case (3), is another possibility. A better understanding of this last mechanism, which is generally active at oxide interfaces, is necessary to identify the true source of interfacial tetragonal SRO symmetry in our samples.

In conclusion, we investigated coherent interfaces between two oxide ferromagnets, LSMO and SRO, of the specific type where an exchange spring is present and governs magnetic switching. The exchange spring enables low-field switching of topologically nontrivial spin textures. In an insulating oxide, such interfacial spin structures would induce electrical polarization like in type II multiferroics. One of the parameters responsible for the formation of the exchange spring is the very strong Mn–O–Ru exchange coupling at the MnO_2 -terminated interface.^[6] The moderate interfacial magnetic anisotropy of SRO required for an exchange spring is suggested to result from a symmetry change of SRO from tetragonal at the interface to orthorhombic away from the interface. Provided there is sufficiently strong exchange coupling (and, if required, a structurally supported anisotropy suppression), other oxide interfaces may show similar interfacial spin structures. For device operation, such interfacial spin structures are a challenge, as they fundamentally alter magnetic switching, exchange bias, and the spin of tunneling electrons, among others. As a promising aspect, they offer a yet little explored terrain for topology-based or magnetoelectric functionalities of oxide interfaces.

3. Experimental Section

LSMO and SRO layers were grown on STO(001) substrates by pulsed laser deposition (PLD) in the sequence of SRO/LSMO/STO(001) using

an excimer laser with 248 nm wavelength and a PLD chamber (Surface GmbH) with high-pressure reflection high-energy electron diffraction (RHEED) facility. The single-crystalline STO substrates were terminated with TiO₂. The growth temperature, laser energy density, and oxygen pressure were 700 °C, 0.3 J cm⁻², and 0.2 mbar, respectively. After growth, samples were annealed for 1 h in oxygen of 200 mbar. Coherent growth of both layers, LSMO and SRO, on STO(001) with in-plane lattice parameter of $a = 3.905 \text{ \AA}$ was confirmed by X-ray diffraction. LSMO–SRO interfaces showed very low intermixing, as characterized by high-resolution scanning transmission electron microscopy (STEM) in a previous study.^[6] Magnetization measurements were carried out in a superconducting quantum interference device (SQUID) magnetometer. The strong diamagnetic contribution was eliminated from field-dependent magnetization $M(H)$ through the following procedure: the high-field slope dM/dH determined between 4 and 5 T was assigned to the diamagnetic susceptibility χ , and $M_{\text{sub}} = \chi H$ was subtracted from magnetization data. (This procedure also eliminated a high-field response from the film.) In temperature-dependent magnetization curves, the constant diamagnetic contribution was determined above 300 K and substrated. The XMCD experiments were carried out at the BL29 BOREAS beamline at the ALBA synchrotron radiation facility. X-ray absorption was measured using circular polarized light with the photon spin parallel (σ^+) or antiparallel (σ^-) with respect to the magnetic field. The field direction was equal to the beam direction. Spectra were collected with the beam in normal incidence (along the pseudocubic 001 direction) and along the 100 in-plane direction with a 20° out-of-plane tilting.^[33] The spectra were recorded using the total electron yield method (by measuring the sample drain current) in a chamber with a vacuum base pressure of 2×10^{-10} mbar at $T = 60 \text{ K}$, after the samples had been cooled in a field of 3 T. The Mn–XMCD hysteresis loops were obtained by measuring, as a function of applied field, the Mn L₃ edge XMCD signal at the energy where the XMCD signal was maximum.

Acknowledgements

The research in Halle was supported by Deutsche Forschungsgemeinschaft, SFB 762 Functional Oxide Interfaces (projects A9 and B1). The authors thank ALBA synchrotron light facility for providing beamtime and technical assistance.

Conflict of Interest

The authors declare no conflict of interest.

Keywords

exchange coupling, exchange spring, interfaces, magnetic films, noncollinear, spin textures

Received: September 29, 2019

Revised: January 2, 2020

Published online: February 6, 2020

- [1] A. Fert, V. Cros, J. Sampaio, *Nat. Nanotechnol.* **2013**, *8*, 152.
 [2] G. Chen, A. K. Schmid, *Adv. Mater.* **2015**, *27*, 5738.
 [3] Q. He, R. Ishikawa, A. R. Lupini, L. Qiao, E. J. Moon, O. Ovchinnikov, S. J. May, M. D. Biegalski, A. Y. Borisevich, *ACS Nano* **2015**, *9*, 8412.
 [4] Z. Liao, M. Huijben, Z. Zhong, N. Gauquelin, S. Macke, R. J. Green, S. Van Aert, J. Verbeeck, G. Van Tendeloo, K. Held, G. Sawatzky, G. Koster, G. Rijnders, *Nat. Mater.* **2016**, *15*, 425.
 [5] D. Kan, R. Aso, R. Sato, M. Haruta, H. Kurata, Y. Shimakawa, *Nat. Mater.* **2016**, *15*, 432.

- [6] S. Das, A. D. Rata, I. V. Maznichenko, S. Agrestini, E. Pippel, N. Gauquelin, J. Verbeeck, K. Chen, S. M. Valvidares, H. B. Vasili, J. Herrero-Martin, *Phys. Rev. B* **2019**, *99*, 024416.
 [7] A. Y. Borisevich, A. R. Lupini, J. He, E. A. Eliseev, A. N. Morozovska, G. S. Svechnikov, P. Yu, Y. H. Chu, R. Ramesh, S. T. Pantelides, S. V. Kalinin, *Phys. Rev. B* **2012**, *86*, 140102(R).
 [8] J. Matsuno, N. Ogawa, K. Yasuda, F. Kagawa, W. Koshibae, N. Nagaosa, Y. Tokura, M. Kawasaki, *Sci. Adv.* **2016**, *2*, e1600304.
 [9] Y. Ohuchi, J. Matsuno, N. Ogawa, Y. Kozuka, M. Uchida, Y. Tokura, M. Kawasaki, *Nat. Commun.* **2018**, *9*, 213.
 [10] L. Wang, Q. Feng, Y. Kim, R. Kim, K. H. Lee, S. D. Pollard, Y. J. Shin, H. Zhou, W. Peng, D. Lee, W. Meng, *Nat. Mater.* **2018**, *17*, 1087.
 [11] F. Y. Bruno, J. Garcia-Barriocanal, M. Varela, N. M. Nemes, P. Thakur, J. C. Cezar, N. B. Brookes, A. Rivera-Calzada, M. Garcia-Hernandez, C. Leon, S. Okamoto, *Phys. Rev. Lett.* **2011**, *106*, 147205.
 [12] D. Preziosi, M. Alexe, D. Hesse, M. Salluzzo, *Phys. Rev. Lett.* **2015**, *115*, 157401.
 [13] S. Okamoto, *Phys. Rev. B* **2010**, *82*, 024427.
 [14] M. Bowen, M. Bibes, A. Barthélémy, J. P. Contour, A. Anane, Y. Lemaitre, A. Fert, *Appl. Phys. Lett.* **2003**, *82*, 233.
 [15] J. A. Mundy, Y. Hikita, T. Hidaka, T. Yajima, T. Higuchi, H. Hwang, D. A. Muller, L. F. Kourkoutis, *Nat. Commun.* **2014**, *5*, 3464.
 [16] P. Yu, J. S. Lee, S. Okamoto, M. D. Rossell, M. Huijben, C. H. Yang, Q. He, J. X. Zhang, S. Y. Yang, M. J. Lee, Q. M. Ramasse, *Phys. Rev. Lett.* **2010**, *105*, 027201.
 [17] E.-J. Guo, J. R. Petrie, M. A. Roldan, Q. Li, R. D. Desautels, T. Charlton, A. Herklotz, J. Nichols, J. van Lierop, J. W. Freeland, S. V. Kalinin, *Adv. Mater.* **2017**, *29*, 1700790.
 [18] X. Ke, M. S. Rzchowski, L. J. Belenky, C.-B. Eom, *Appl. Phys. Lett.* **2004**, *84*, 5458.
 [19] M. Ziese, I. Vrejoiu, E. Pippel, P. Esquinazi, D. Hesse, C. Etz, J. Henk, A. Ernst, I. V. Maznichenko, W. Hergert, I. Mertig, *Phys. Rev. Lett.* **2010**, *104*, 167203.
 [20] A. Solignac, R. Guerrero, P. Gogol, T. Maroutian, F. Ott, L. Largeau, P. Lecoeur, M. Pannetier-Lecoeur, *Phys. Rev. Lett.* **2012**, *109*, 027201.
 [21] S. Das, A. Herklotz, E. Pippel, E. J. Guo, D. Rata, K. Dörr, *Phys. Rev. B* **2015**, *91*, 134405.
 [22] X. Ke, L. J. Belenky, V. Lauter, H. Ambaye, C. W. Bark, C. B. Eom, M. S. Rzchowski, *Phys. Rev. Lett.* **2013**, *110*, 237201.
 [23] J. H. Kim, I. Vrejoiu, Y. Khaydukov, T. Keller, J. Stahn, A. Rühm, D. K. Satapathy, V. Hinkov, B. Keimer, *Phys. Rev. B* **2012**, *86*, 180402(R).
 [24] A. V. Ramos, J. B. Moussy, M. J. Guittet, M. Gautier-Soyer, C. Gatel, P. Bayle-Guillemaud, B. Warot-Fonrose, E. Snoeck, *Phys. Rev. B* **2007**, *75*, 224421.
 [25] B. Li, R. V. Chopdekar, E. Arenholz, A. Mehta, Y. Takamura, *Appl. Phys. Lett.* **2014**, *105*, 202401.
 [26] G. Koster, L. Klein, W. Siemons, G. Rijnders, J. S. Dodge, C. B. Eom, D. H. Blank, M. R. Beasley, *Rev. Mod. Phys.* **2012**, *84*, 253.
 [27] N. Nagaosa, X. Z. Yu, Y. Tokura, *Philos. Trans. R. Soc. A* **2012**, *370*, 5806.
 [28] H. Katsura, N. Nagaosa, A. V. Balatsky, *Phys. Rev. Lett.* **2005**, *95*, 057205.
 [29] A. Herklotz, K. Dörr, *Eur. Phys. J. B* **2015**, *88*, 60.
 [30] A. Vailionis, W. Siemons, G. Koster, *Appl. Phys. Lett.* **2008**, *93*, 051909.
 [31] A. Herklotz, A. T. Wong, T. Meyer, M. D. Biegalski, H. N. Lee, T. Z. Ward, *Sci. Rep.* **2016**, *6*, 26491.
 [32] M. Ziese, I. Vrejoiu, E. Pippel, A. Hähnel, E. Nikulina, D. Hesse, *J. Phys. D* **2011**, *44*, 345001.
 [33] S. Agrestini, Z. Hu, C. Y. Kuo, M. W. Haverkort, K. T. Ko, N. Hollmann, Q. Liu, E. Pellegrin, M. Valvidares, J. Herrero-Martin, P. Gargiani, *Phys. Rev. B* **2015**, *91*, 075127.